Icarus 266 (2016) 15–23

Contents lists available at ScienceDirect

Icarus

journal homepage: www.journals.elsevier.com/icarus

On the detection of carbon monoxide as an anti-biosignature in exoplanetary atmospheres

Yuwei Wang [a], Feng Tian [b,c,*], Tong Li [b], Yongyun Hu [a]

[a] Laboratory for Climate and Ocean-Atmosphere Sciences, Department of Atmospheric and Oceanic Sciences, School of Physics, Peking University, Beijing 100871, China
[b] Ministry of Education Key Laboratory for Earth System Modeling, Center for Earth System, Science, Tsinghua University, Beijing 100084, China
[c] Joint Center for Global Change Studies (JCGCS), Beijing 100875, China

ARTICLE INFO

Article history:
Received 6 August 2015
Revised 12 October 2015
Accepted 9 November 2015
Available online 17 November 2015

Keyword:
Astrobiology
Extra-solar planets
Radiative transfer
Search for Extraterrestrial Life

ABSTRACT

Recent works suggest that oxygen can be maintained on lifeless exoplanets in the habitable zones of M dwarfs as the results of photochemical reactions. However, the same photochemical models also predict high concentrations of carbon monoxide (CO) in the corresponding atmospheres. Here we use a line-by-line radiative transfer model to investigate the observation requirements of O_2 and CO in such atmospheres. The results show that photochemically produced CO can be readily detected at 1.58, 2.34, and 4.67 μm. We suggest that future missions aiming at characterization of exoplanetary atmospheres consider detections of CO as an anti-biosignature.

1. Introduction

Earth-sized rocky planets are common in the habitable zones of M dwarfs (Dressing and Charbonneau, 2013, 2015; Gaidos, 2013; Kopparapu, 2013; Tuomi et al., 2014). Although most observation feasibility considerations favor M dwarfs as the most promising targets in the search for habitable exoplanets and life in the near future, atmospheric composition of habitable exoplanets are strongly affected by the unique UV spectra of M dwarfs (France et al., 2012, 2013; Hu et al., 2012; Tian et al., 2014; Domagal-Goldman et al., 2014; Luger and Barnes, 2015; Gao et al., 2015; Harman et al., 2015). In particular, atmospheres with 5% CO_2 on abiotic Earth-mass planets with Earth-like climate around M dwarfs could contain 10^{-3} level of O_2 as a consequence of slow photolysis of H_2O and H_2O_2 (Tian et al., 2014; Harman et al., 2015). If the atmospheres are dominated by CO_2 and the exoplanets are desiccated because of early stellar luminosity evolution (Ramirez and Kaltenegger, 2014; Tian and Ida, 2015; Luger and Barnes, 2015), atmospheric oxygen could even reach 1–10% (Gao et al., 2015). Interestingly the CO contents in these hypothetical atmospheres are always on the same order of magnitude as that of O_2: 10^{-3} in Tian et al. (2014) and 1–10% in Gao et al. (2015).

CO can act as an energy source for some microbes on the Earth (Walker, 1977; Des Marais, 1998; House et al., 2003; Battistuzzi et al., 2004). It is estimated that CO deposition velocity on an abiotic Earth would have been on the order of 10^{-8}–10^{-9} cm/s, 4 or 5 orders of magnitude lower than that after the development of acetogens (Kharecha et al., 2005) – it is more difficult for CO to accumulate in the atmosphere of an inhabited planet. Thus detection of high level of atmospheric CO may be regarded as an anti-biosignature. A somewhat weaker statement has also been proposed: the lack of some species which should be present due to natural processes, such as CO through photochemistry on M dwarf exoplanets, could also be a biosignature (Eric Gaidos, private communication). Thus the detection of CO itself could be interesting for atmosphere characterization of habitable zone rocky exoplanets around M dwarfs.

Whether the high atmospheric oxygen and CO contents are observable by future exoplanetary atmosphere characterization missions/facilities is one question we aim to address in this work. In Section 2, we introduce the radiation transfer model (LT model) used in this work. Results are shown in Section 3. In Section 4, we estimate the observation time needed to resolve O_2 and CO predicted to exist in the atmospheres of habitable zone rocky planets of M dwarfs. Conclusion are summarized in Section 5.

2. Model description

The LT model (Li and Tian, 2012) is a line-by-line model developed to calculate the transmission, reflection, and emission spectra of exoplanets. It uses the line intensities and half-widths

* Corresponding author at: Ministry of Education Key Laboratory for Earth System Modeling, Center for Earth System, Science, Tsinghua University, Beijing 100084, China.

http://dx.doi.org/10.1016/j.icarus.2015.11.010
0019-1035/

(both self-broadening and air-broadening) from the HITRAN2012 database (Rothman et al., 2013). Voigt line shape profiles are used for all gases with cut-off distances set to 50 times Voigt half-widths from line centers. An incidence and reflection angles of 60° in a plane-parallel atmosphere are used to approximate the geometry integration of exoplanets, consistent with the approaches in previous works (Des Marais et al., 2002; Kaltenegger et al., 2007).

The default resolution of the LT model is 0.01 cm^{-1} between 0.5 and 10 μm, corresponding to $R = \lambda/\Delta\lambda = 2 \times 10^6$ and 10^5 at 0.5 and 10 μm respectively, adequate to resolve all major absorption lines in the HITRAN2012 database. In comparison, the High Resolution Echelle Spectrometer (HIRES) of Keck I Telescope has R = 25,000–85,000 at 0.3–1 μm (Vogt et al., 1994; Oke et al., 1995), with the range based on the choice of slit plate in observations. The Low Resolution Imaging Spectrometer (LRIS) of Keck I Telescope has R = 300–5000 at 0.3–1 μm. The Near-Infrared Spectrograph (NIRSPEC) of Keck II Telescope has R = 25,000 and 2500 at 0.95–5.5 μm (McLean et al., 1998). The moderate and low resolutions of James Webb Space Telescope (JWST) are R = 1000 and 100 between 0.6 and 5.0 μm (Wright et al., 2004; Bagnasco et al., 2007). All results shown here are R = 100 spectra smoothed from high resolution LT spectra.

The main absorption bands of O_2 are 0.69 μm (B band), 0.76 μm (A band), and 1.27 μm. Even with a low concentration (~0.1 ppmv) in the Earth's atmosphere, CO can be recognized at 4.67 μm and 2.34 μm (Fig. 3.1 in Goody and Yung, 1989). CO 1.58 μm feature is invisible at the surface of the Earth with 50 cm^{-1} spectral resolution (corresponds to roughly R = 128) (Liou, 2002). The non-detection of CO 1.58 μm feature is partially due to the weakness of this absorption band and partially due to the overlapping CO_2 absorption. For exoplanets the concentration of CO could be much greater than that in the Earth's atmosphere. Thus CO 1.58 μm absorption band is included in this study. For exoplanets at Earth-equivalent distances, the emission from the planets far exceeds the reflected stellar radiation near 5 μm. To take this effect into consideration, the calculated planetary emission spectrum at the top of the atmosphere (TOA) is divided by the incident stellar spectrum and the ratio is included in the reflectivity calculations. The incident stellar spectrum is a blackbody spectrum at 3500 K with the total energy flux scaled to 1360 W/m^2, the solar constant of modern Earth (Kopp and Lean, 2011). Note that this incident flux is only used to calculate the reflection spectrum.

For simplicity purpose, a wavelength dependent planetary surface albedo, which includes the combined effects of clouds, aerosols, and surface type, is used in this work. Based on observations of the Earth (Jin et al., 2014; Turnbull et al., 2006), the surface albedo is set to 0.28 for 0.6–1.1 μm, 0.26 for 1.1–1.4 μm, 0.21 for 1.4–1.8 μm, and 0.17 for 1.8–2.4 μm, respectively. The NIR spectrum of the Earth calculated by the LT model with these surface albedo and modern Earth atmospheric composition profiles resembles the observed globally averaged reflectance spectrum (Jin et al., 2014). Observations for 4.5–5 μm is scarce. Considering the surface types and cloud scattering properties, a surface albedo of 0.15 is used. Our results are insensitive to this assumption. For planets with Earth-like climate, planetary emission dominates in this wavelength range. For desiccated exoplanets, 1.58 and 2.34 μm are the best wavelengths for CO detection. The lack of water vapor makes CO features more obvious in 2.34 μm. Thus setting 0.15 albedo for 4.5–5 μm should not significantly change the detectability of CO.

For exoplanets with Earth-like climate, the mixing ratios of CO_2, CO, and O_2 (altitude-independent) are set to 5%, 0.5%, and 0.2% respectively based on Tian et al. (2014). The temperature and H_2O profiles are also from Tian et al. (2014). For desiccated

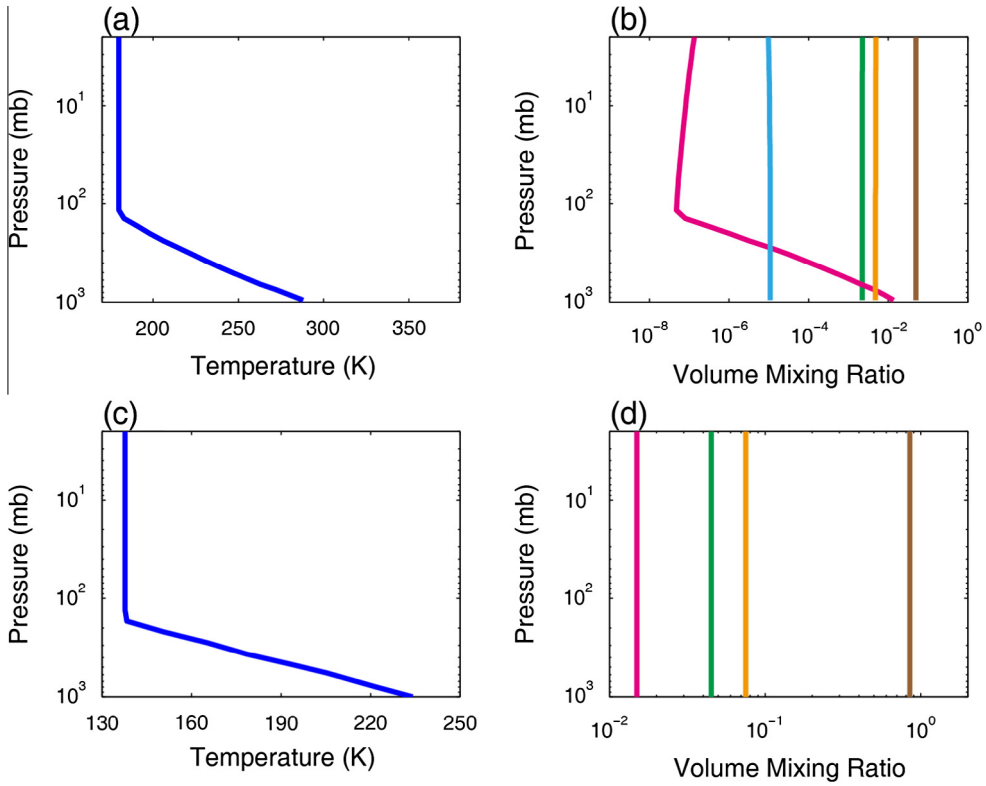

Fig. 1. Temperature and composition profiles in Tian et al. (2014) (panel a, panel b) and in Gao et al. (2015) (panel c, panel d). The green, orange, pink, brown, and light blue curves in panel b and d represent O_2, CO, H_2O, CO_2 and CH_4 respectively. The H_2O mixing ratio in panel d is multiplied by 10^5. The H_2O contents are far blow saturation and thus its mixing ratio is constant in the lower atmosphere. (For interpretation of the references to color in this figure legend, the reader is referred to the web version of this article.)

exoplanets, the mixing ratios of CO_2, CO, O_2, and surface H_2O in case 1 of Gao et al. (2015) are 85%, 7.5%, 4.5%, and 1.5×10^{-7} respectively. In case 6 of Gao et al. (2015) these values are 50%, 30%, 15%, and 4×10^{-11} respectively. The concentrations of CO and O_2 in case 6 of Gao et al. (2015) are greater and should be easier to detect. Here only the spectra and integration time for case 1 in Gao et al. (2015), which is more difficult to observe, are shown.

The surface temperature in Gao et al. (2015) is <240 K, which is used as the base case for the desiccated exoplanets. For completeness purpose, sensitivity tests (not shown) are carried out with Earth-like temperature profiles for the desiccated exoplanets and most of the results are similar except for the emission ratio at 4.67 μm which is highly related to the temperature. Higher temperature makes observation more easily in this band. Thus our results for reflectivity are robust all through different climate regimes in the habitable zone. The absorbing gases are O_2, CO, CO_2, CH_4, and H_2O in Tian et al. (2014), and O_2, CO, CO_2, and H_2O in Gao et al. (2015). Temperature and composition profiles in Tian et al. (2014) and in case 1 of Gao et al. (2015) are shown in Fig. 1.

3. NIR spectra in absorption bands of O_2 and CO

For exoplanets with Earth-like climate around M dwarfs, the reflection spectra near the O_2 and CO absorption bands are shown in Fig. 2. The blue solid curves are from calculations with all absorbing gases included. The red dashed curves in the left panels of Fig. 2 are the results without O_2. The signal of O_2 is strongest at 0.76 μm (reflectivity decreased from 0.28 to 0.25, Fig. 2b), followed by 0.69 μm (Fig. 2a) and 1.27 μm (Fig. 2c). At high spectral resolution (R = 1000 and 10,000) the signal of 10^{-3} level of O_2 is stronger (Fig. 3). Note that the two weaker features of O_2 overlap with absorption features of H_2O and CO_2, while the 0.76 μm feature of O_2 avoids interferences with other major species.

The reflection spectra at the 3 CO absorption bands are shown in the right panels of Fig. 2 (blue and red curves are with and without CO respectively). CO overlaps with CO_2 near 1.58 μm and the presence of 10^{-3} level of CO leads to a small decrease of reflectivity (~0.02) at 1.56 and 1.59 μm (Fig. 2d). CO overlaps with H_2O and CH_4 near 2.34 μm. Although the absorption of H_2O and CH_4 in the modeled atmosphere of Tian et al. (2014) decreases the planetary reflectivity to between 0.05 and 0.1 in this band, the presence of 10^{-3} level of CO further decreases the reflectivity to almost 0 (Fig. 2e). CO overlaps with H_2O and CO_2 near 4.67 μm. H_2O absorption becomes strong at $\lambda > 4.9$ μm. At 5% atmospheric CO_2 level, the absorption of CO_2 leads to near-zero reflectivity at 4.2–4.4 and 4.7–4.8 μm (Fig. 2f). In between the absorption bands of H_2O and CO_2 there is a detection window for CO (4.5–4.7 μm), where the presence of 10^{-3} level of CO decreases the reflectivity from 0.6 to near zero (Fig. 2f).

The higher O_2 contents on desiccated exoplanets (case 1 in Gao et al., 2015) produce stronger O_2 absorption signals (Fig. 4a–c). In addition, the lack of atmospheric H_2O makes the O_2 signal at 0.69 μm (Fig. 4a) more apparent. Although the atmospheres used in the calculations contain 85% CO_2, the signal of O_2 at 1.27 μm (Fig. 4c) is still stronger than that in Fig. 2c. Similarly the absence of H_2O and a higher CO concentration on desiccated exoplanets lead to stronger signals of CO at 1.56 and 1.59 (Fig. 4d), 2.34 (Fig. 4e), and 4.6 μm (Fig. 4f). In addition, the reflectivity change due to the absorption of CO can be seen between 4.9 and 5.0 μm on desiccated exoplanets (Fig. 4f), whereas it is almost invisible for exoplanets with Earth-like climate.

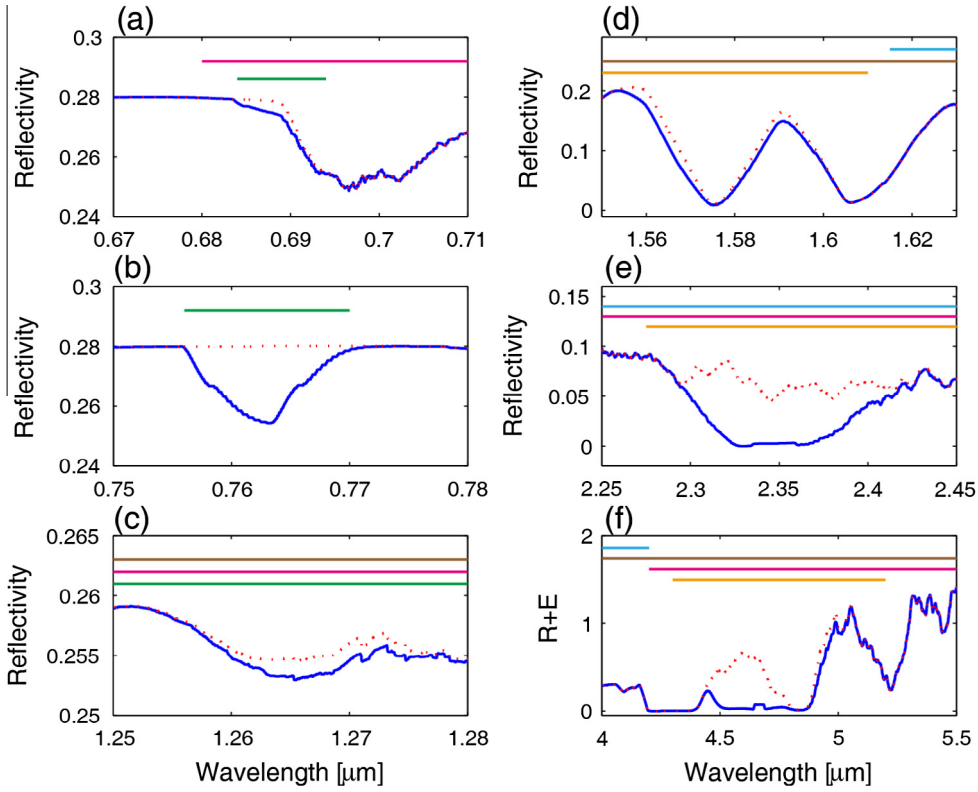

Fig. 2. (a–e) Reflectivity as functions of wavelength with spectral resolution of R = 100. (f) The sum of reflection and planetary emission as a function of wavelength with R = 100. The blue solid curves represent results from composition profiles are from Tian et al. (2014). The red dashed curves represent results without O_2 for (a–c) or CO for (d–f). The straight lines in green, orange, pink, brown, and light blue indicate strong absorption bands for O_2, CO, H_2O, CO_2, and CH_4 respectively. (For interpretation of the references to color in this figure legend, the reader is referred to the web version of this article.)

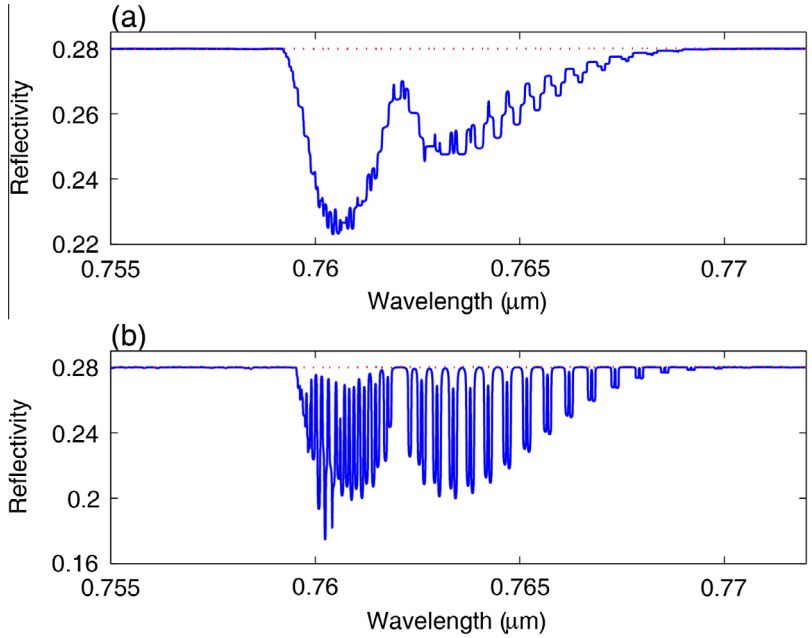

Fig. 3. High resolution reflection spectra near 0.76 μm. The blue curves show the results with all gases in Fig. 1 and the red dotted lines represent the results without oxygen. (a) Resolution R = 1000. (b) Resolution R = 10,000. (For interpretation of the references to color in this figure legend, the reader is referred to the web version of this article.)

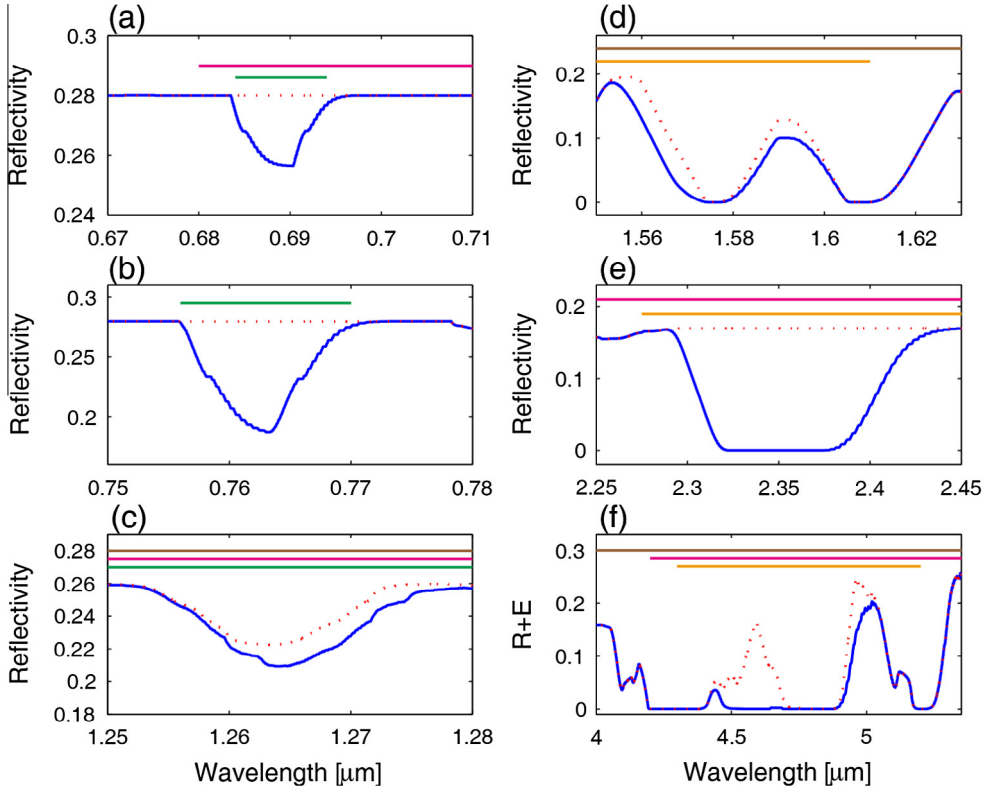

Fig. 4. The same with Fig. 2 except that the temperature and composition profiles are from case 1 in Gao et al. (2015).

4. Discussions

4.1. Observation time

To estimate the observation time needed to identify O_2 and CO, we follow the assumptions in Rein et al. (2014): (1) photons from the star is reduced to negligible level; (2) a quadrature position for the exoplanet; (3) the star-facing side of the planet reflects and emits uniformly; (4) all noises other than the photon noise are negligible; (5) the photon noise satisfies a Poisson distribution. With two extra assumptions: (1) the efficiency of telescope and the spectrograph are ~100%; and (2) the stellar spectrum is close to that of a black body, a relationship between the observation time Δt, the wavelength dependent reflectivity A, the signal to noise

Table 1
Typical values for t_0 in Eq. (1).

λ (μm)	Stellar temperature (K)						
	3000	3500	4000	4500	5000	5500	6000
0.69	1.61	1.10	0.89	0.79	0.76	0.75	0.77
0.76	1.13	0.85	0.73	0.69	0.68	0.70	0.74
1.27	0.41	0.43	0.48	0.55	0.64	0.74	0.86
1.58	0.37	0.43	0.51	0.61	0.74	0.88	1.05
2.34	0.40	0.53	0.69	0.88	1.12	1.39	1.71
4.67	0.85	1.24	1.74	2.37	3.13	4.03	5.11

Table 2
Observation time for detection of O_2 and CO.

Exoplanets with Earth-like climate				
λ (μm)	A with O_2	A without O_2	SNR	Δt (h)
0.69	0.274	0.279	112	148
0.76	0.254	0.28	22	4.3
1.27	0.253	0.255	255	329
λ (μm)	A with CO	A without CO	SNR	Δt (h)
1.58	0.175	0.2	16	1.7
2.34	0.01	0.08	3	0.1
4.67	0.03	0.66	3	0.024
Desiccated exoplanets				
λ (μm)	A with O_2	A without O_2	SNR	Δt (h)
0.69	0.256	0.28	24	6.4
0.76	0.19	0.28	7	0.35
1.27	0.21	0.223	35	6.8
λ (μm)	A with CO	A without CO	SNR	Δt (h)
1.58	0.155	0.195	10	0.62
2.34	0	0.17	2	0.04
4.67	0	0.16	2	0.1

ratio SNR, and the spectral resolution R is derived based on Eq. (5) in Rein et al. (2014):

$$\Delta t = t_0 \left(\frac{A}{0.3}\right)^{-1} \left(\frac{r_p}{r_E}\right)^{-2} \left(\frac{F_*}{1367}\right)^{-1} \left(\frac{d}{10\,\mathrm{pc}}\right)^{2} \left(\frac{D}{6.5\,\mathrm{m}}\right)^{-2} \left(\frac{\mathrm{SNR}}{10}\right)^{2} \left(\frac{R}{100}\right) \quad (1)$$

where r_p and r_E are the radii of the exoplanet and the Earth, F_* the energy flux received by the planet in unit of W/m^2, d the distance between the exoplanet and the Earth, and D the telescope diameter in meter. t_0 is defined as

$$t_0 = 6.87 \times 10^{-15} \times \frac{T_*^4}{\lambda^2 B(T_*, \lambda)} \quad \text{hours} \quad (2)$$

where T_* is the temperature of the star, $B(T_*, \lambda)$ is the black body plank function at wavelength λ and temperature T_*. $\frac{B(T_*,\lambda)}{T_*^4}$ is proportional to the ratio between the energy flux around λ and the total stellar energy flux. One of the two λ's in the denominator is from the expression of the spectral resolution ($\lambda/\Delta\lambda$), and the other from the energy of photons (hc/λ). The values of t_0 for typical T_* and λ are shown in Table 1.

The real situations are certainly more complicated and the assumptions in the derivation of Eq. (1) may not be satisfied. Nevertheless, Eq. (1) can be used to estimate the feasibility of O_2 and CO detection in exoplanetary atmospheres. In the following we assume that in order to distinguish an atmosphere with O_2 and/or CO from one without, an SNR corresponding to half of the reflectivity decrease caused by the presence of O_2 or CO is needed. For example, the reflectivity decrease at 0.69 μm due to the presence of O_2 on Earth-like climate exoplanets is 0.005. Thus SNR = 0.279/(0.005/2) = 112. Observation time based on this criteria will guarantee the detection of O_2 or/and CO at the concentration levels predicted by photochemical models. Using this

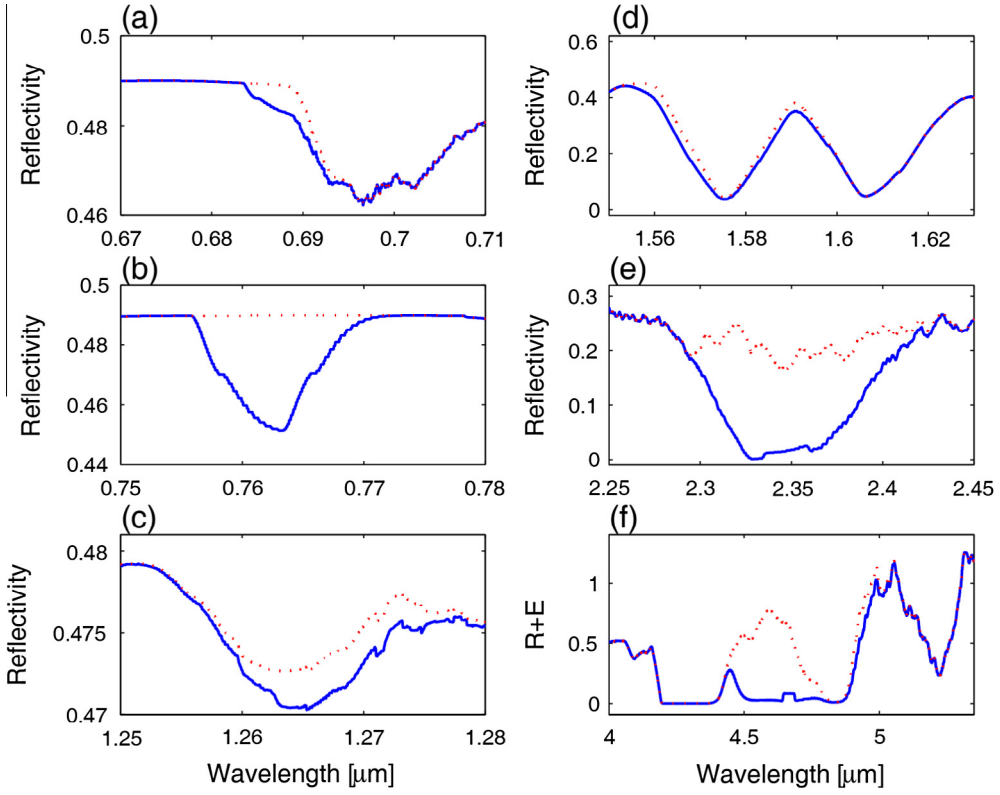

Fig. 5. Similar to Figs. 2 and 4 but a dense cloud layer with 50% cloud fraction and 0.7 albedo at 2 km is added in the LT model.

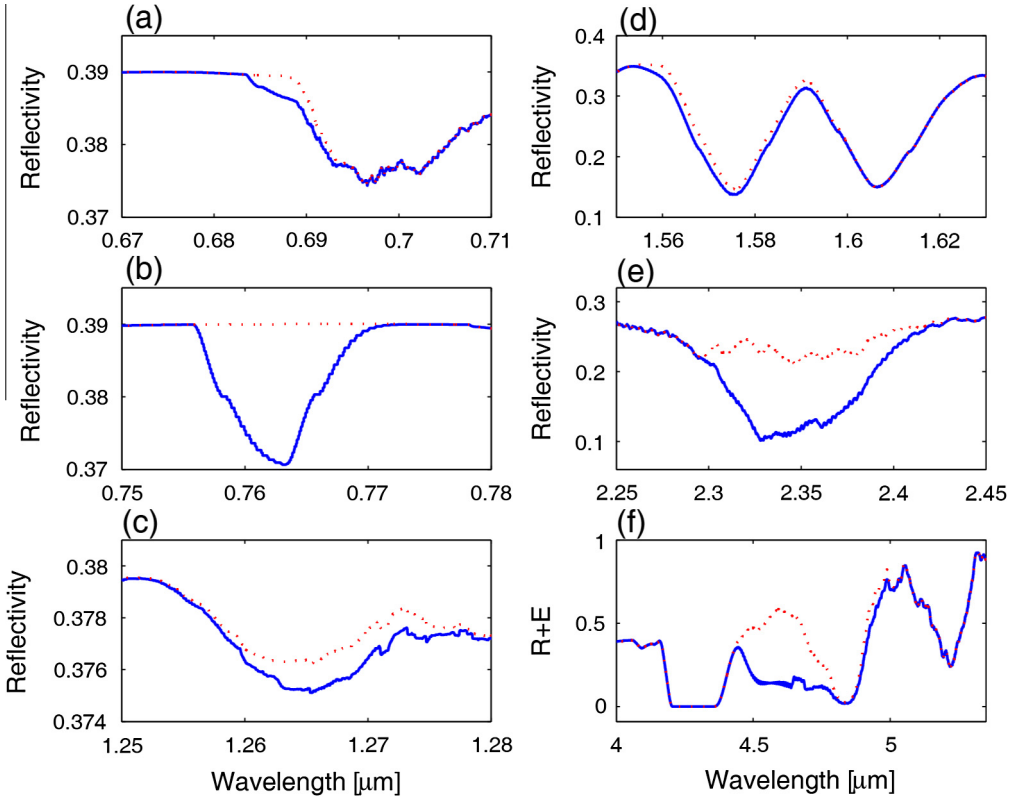

Fig. 6. Similar to Figs. 2 and 4 but a dense cloud layer with 50% cloud fraction and 0.5 albedo at 10 km is added in the LT model.

requirement, the observation time needed for O_2 and CO detection on habitable zone exoplanets around M dwarfs with 3500 K surface temperature located at 10 pc by a 6.5-m telescope are listed in Table 2.

For exoplanets with Earth-like climate, the detections of 10^{-3} level of O_2 at 0.69 and 1.27 μm require large SNR and thus long observation time. Thus 0.76 μm will be the best option for O_2 detection. The observation time for CO detection is rather short, consistent with a greater reflectivity reduction caused by similar amount of CO than by O_2.

GCM simulations indicate that the bond albedo of synchronously rotating habitable exoplanets at Earth equivalent distance around M dwarfs is ~0.46, greater than that of the Earth because of greater cloud coverage (Yang et al., 2013), which can decrease the observation time. On the other hand, the effective column density of absorbing gas above the clouds is smaller, which could lead to a weaker signal of the gas and increase the observation time. Two sensitivity tests were carried out for the Earth-like climate exoplanets assuming clouds at 2 and 10 km respectively. The albedo of clouds at 2 and 10 km are set to 0.7 and 0.5 respectively (Fig. 5.9 in Pierrehumbert, 2010), and the cloud fractions are set to 50% for both. The results are shown in Figs. 5 and 6 respectively. The existence of clouds at 2 km makes the features stronger and decreases the observation time by 30%, 60%, and 70% at 0.76, 1.58, and 2.34 μm respectively. The existence of clouds at 10 km increases the observation time at 0.76 and 1.58 μm by a factor of 1.3 and 1.7 but decrease the observation time at 2.34 μm by 10%. Real cloud distributions and characteristics in exoplanetary atmospheres are certainly much more complicated. But the observation time for CO detection does not appear to be prohibitively long.

The observed spectrum of AD Leo (Segura et al., 2005), when scaled to a total energy flux of 1360 W/m^2, contains absorption

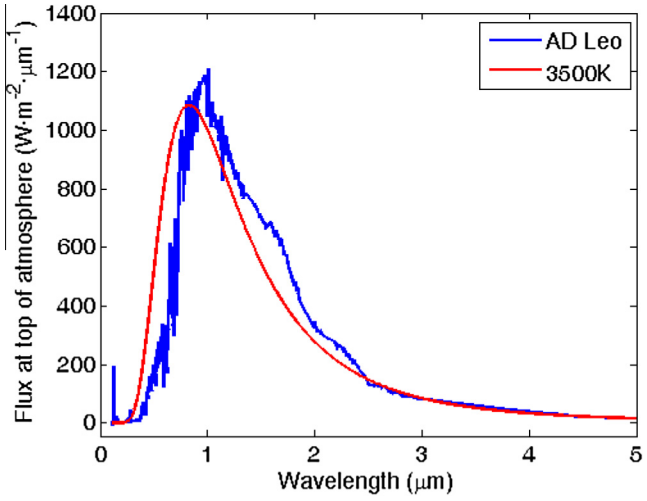

Fig. 7. 3500 K black body spectrum (red line) and observed M dwarf AD Leo spectrum (blue line). Both spectra are scaled to have a total energy flux of 1360 W/m^{-2}. (For interpretation of the references to color in this figure legend, the reader is referred to the web version of this article.)

features at $\lambda < 1$ μm, enhanced fluxes at 1–2.5 μm and similar fluxes at $\lambda > 2.5$ μm when compared to a blackbody spectrum at 3500 K (Fig. 7). Thus the observation time for the first 2 CO bands in Table 2 could be overestimated for exoplanets at Earth equivalent distances around M dwarfs.

A unity emissivity is assumed in calculating the planetary emission spectra. Considering a 0.15 surface reflectivity, the corresponding surface emissivity should be 0.85. Thus the observation time at 4.67 μm could be underestimated by ~10%.

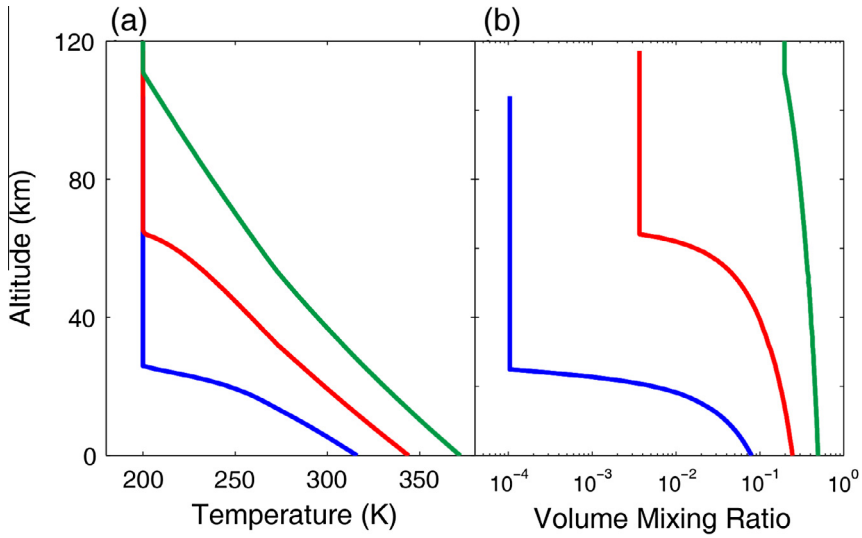

Fig. 8. (a) Temperature profiles with surface temperature fixed at 316 (blue), 344 (red), and 372 K (green) respectively. An atmosphere with higher surface temperature contains more water vapor and thus the more efficient latent heat release reduces the lapse rate to a lower value. (b) Corresponding water vapor mixing ratio profiles assuming unity relative humidity. (For interpretation of the references to color in this figure legend, the reader is referred to the web version of this article.)

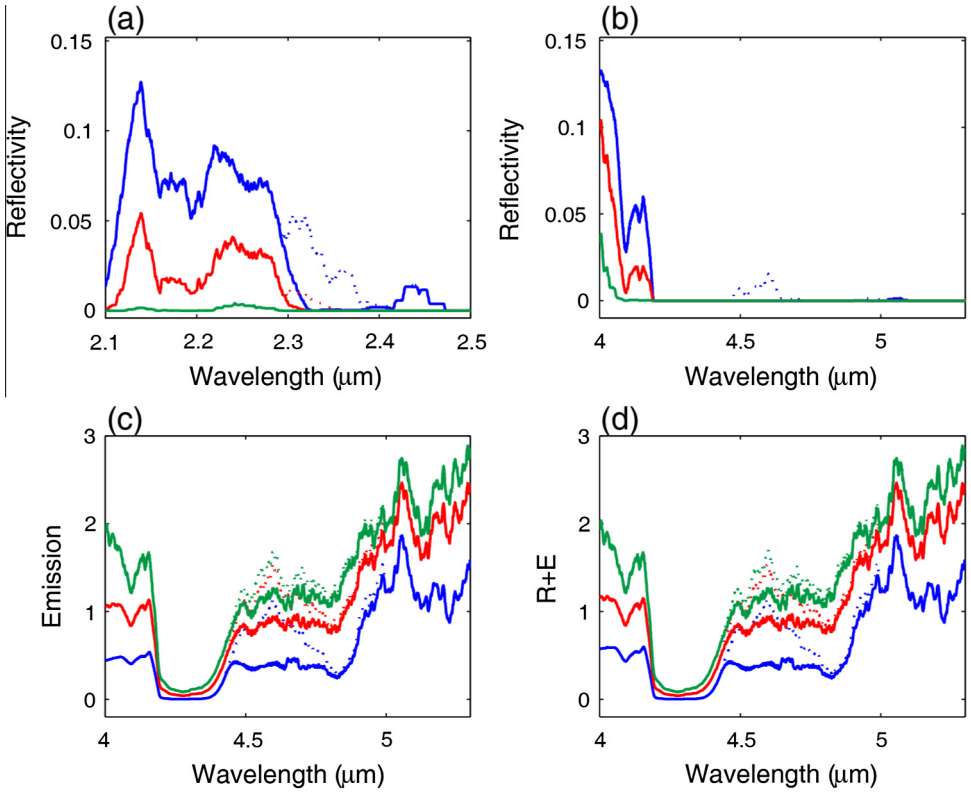

Fig. 9. Reflection, emission, and combined (reflection + emission) spectra (R = 100) at 2.34 (a) and 4.67 μm (b–d) for warm exoplanets. The dashed curves represent results with atmospheric composition profiles in Tian et al. (2014) but with different profiles of temperature (Fig. 8) and H_2O (see the main text). The solid curves are results without CO. The blue, red, and green curves correspond to surface temperature of 316, 344, and 372 K respectively. (For interpretation of the references to color in this figure legend, the reader is referred to the web version of this article.)

4.2. Warm exoplanets

Some absorption features of O_2 and CO overlap with H_2O absorption bands. Because atmospheric H_2O content increases strongly with temperature, a planet with higher surface and atmospheric temperature could have atmospheric H_2O concentration high enough to affect the detection of CO and O_2. In order to check this effect, sensitivity tests are carried out with elevated surface temperatures and corresponding atmospheric temperature profiles which are adjusted according to moist adiabatic process that includes both the cooling from air parcel expansion and the heating from water vapor latent heat release (Chapter 2.7.2 in Pierrehumbert, 2010). Including the latent heat reduces the lapse rate from 9.8 K/km to 6.5 K/km on the Earth. To maximize the absorption effect of H_2O, the relative humidity in the troposphere of the sensitivities tests (T_s = 316, 344, 372 K) are assumed to unity.

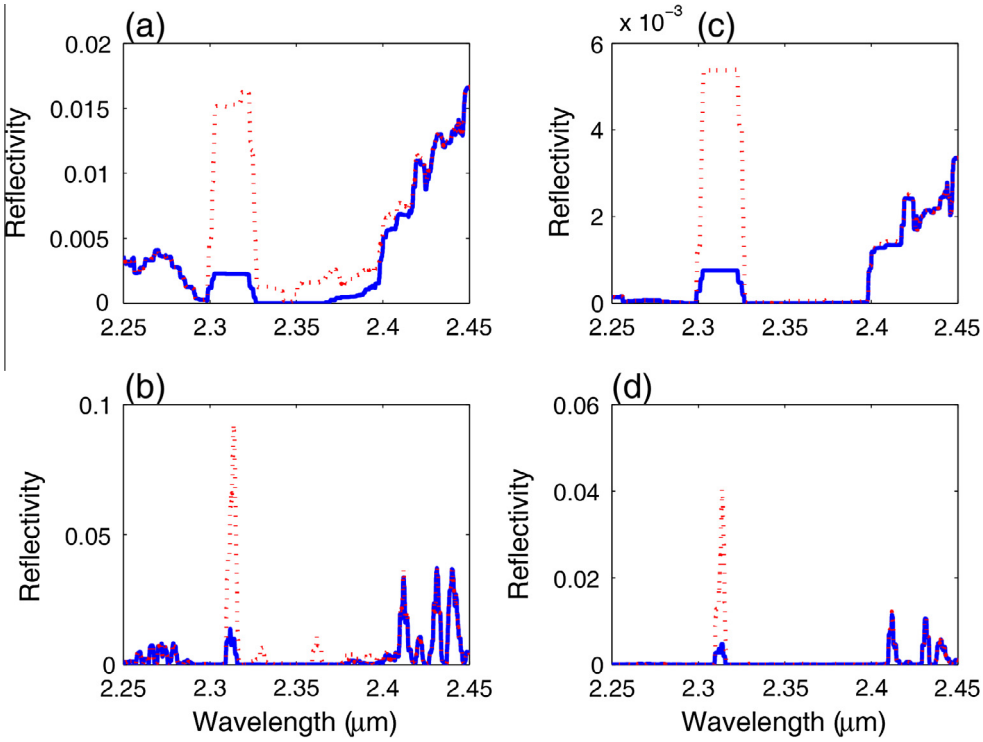

Fig. 10. Reflection spectra near 2.34 μm for exoplanetary atmospheres with 300 (panels a and b) and 1000 (panels c and d) ppmv of CH_4. The spectral resolutions are $R = 100$ for panels a and c, $R = 1000$ for panels b and d. The blue solid curves are results with composition profiles in Fig. 1. The red dashed curves represent results without CO. (For interpretation of the references to color in this figure legend, the reader is referred to the web version of this article.)

The corresponding surface H_2O mixing ratios are 8%, 25%, and 49% respectively. The surface dry air pressure is held at 1 bar dry background gas. It can be seen that from Fig. 8 that the lapse rates are much smaller than that in the Earth's troposphere because of the large water vapor content. In reality warm exoplanets could have relative humidity <1, which would have less shielding effect on CO detection than studied here. Thus these sensitivity tests present overestimates of the observation times required for CO detection. The mixing ratio profiles of all other species are held identical to those in Tian et al. (2014).

Fig. 9a shows the reflectivity at 2.34 μm with resolution of $R = 100$ for the 3 sensitivity tests. The CO signal weakens but is still recognizable for 316 and 344 K surface temperature cases (observation time are 0.13 and 0.64 h respectively). Fig. 3b–d shows the reflectivity, emission, and combined spectra near 4.67 μm for warm exoplanets. CO signal is only recognizable in the reflection spectrum in the 316 K case (Fig. 9b). However, planetary emission far exceeds the reflection in these high temperature cases (Fig. 9c) and thus the presence of CO can be observed in the combined spectra even in the case of 372 K surface temperature (Fig. 9d). The observation time is less than 0.15 h for all 3 high temperature cases.

Note that a surface temperature of 340 K corresponds to the transition into a moist runaway state (Kasting et al., 1993) and a rapid loss of water could start when surface temperature reaches 350 K (Wolf and Toon, 2015). An observational constraint on the surface and atmospheric temperature profile, which should be required for the confirmation of the habitability of an exoplanet, will significantly help the detection of CO and biosignature on exoplanets near the inner edge of the habitable zones.

4.3. High level CH_4

CH_4 has both biological and non-biological sources. CH_4 content is on the order of 10 ppmv in Tian et al. (2014) but could be significantly higher even on abiotic exoplanets (Segura et al., 2005; Rugheimer et al., 2015). As discussed earlier, CH_4's absorption features partially overlaps with that of CO at 2.34 μm. LT model calculations with $R \sim 100$ show that the presence of 300 ppmv and 1000 ppmv CH_4 on an exoplanet with Earth-like climate would reduce reflectivity near 2.34 μm to 0.015 and 0.005 respectively (Fig. 10a and c). Although the presence of 10^{-3} level of CO can still reduce the reflectivity further and the idealized observation time are only 0.5 and 2.2 h for 300 and 1000 ppmv of CH_4 respectively, weak reflection signals from the exoplanets will place stronger requirements to instrument noise and stellar light reduction. At higher spectral resolution ($R = 1000$) the detailed absorption features of CH_4 are revealed (Fig. 10b and d) and the signals of CO near 2.34 μm is more prominent. But the corresponding observation time are increased to 10 and 18 h for 300 and 1000 ppmv of CH_4 respectively.

The above analysis show that the real difficulty for CO detection is that CO NIR absorption bands overlap with those of CO_2, H_2O, and CH_4, which could all be present in terrestrial exoplanetary atmospheres. Distinguishing the absorption signals of CO in such atmospheres probably will require simultaneous observations at 1.58, 2.34, and 4.67 μm, as well as the characteristic absorption bands of CO_2, H_2O, and CH_4. Although the short observation time for CO detection is only indicative, careful planning for instruments should be useful to ensure successful detection of O_2 and CO and other important absorbing gases in exoplanetary atmospheres.

5. Conclusion

In this work, a line-by-line radiative transfer model (the LT model) is used to calculate the reflection and emission NIR spectra of habitable zone Earth-mass exoplanets around M dwarfs in order to investigate the detectability of O_2 and CO in the corresponding atmospheres. Two scenarios are considered: planets with Earth-like climate and desiccated planets. The LT model calculations show that

(1) 10^{-3} level of photochemically produced O_2 is detectable at 0.76 μm, in agreement with the findings in previous works (Kaltenegger et al., 2007; Rodler and López-Morales, 2014);
(2) 10^{-3} level of CO in the corresponding atmospheres is also detectable at NIR absorption bands (1.58, 2.34, and 4.67 μm);
(3) The optimistic estimate on JWST observation time needed for exoplanets with Earth-like climate are 4.3 h at 0.76 μm for O_2 detection and 1.7, 0.1, 0.03 h at 1.58, 2.34 and 4.67 μm for CO detection. On desiccated planets the observation time are much less.

Thus simultaneous observations of O_2 and CO are feasible and will be useful to distinguish true biosignature (O_2 without CO) from photochemically produced false positive biosignature (O_2 + CO). We suggest that simultaneous observations of O_2 and CO be considered by future exoplanet atmosphere characterization observations.

Acknowledgments

We thank two anonymous reviewers for constructive comments. Y.W. and Y.H. are supported by the National Natural Science Foundation of China (41025018 and 41375072). F.T. and T.L. are supported by the National Natural Science Foundation of China (41175039), the Startup Fund of the Ministry of Education of China, and the Tsinghua University Initiative Science Research Program. F. T. thanks the host of NCAR-HAO during preparation of the original manuscript. Y.W. thanks helpful discussion with F. Yan. This research uses the Exoplanet Orbit Database and the Exoplanet Data Explorer at exoplanets.org. All calculations were performed on the supercomputer at the LaCOAS of Peking University.

References

Bagnasco, G. et al., 2007. Overview of the Near-Infrared Spectrograph (NIRSpec) instrument on-board the James Webb Space Telescope (JWST). Opt. Eng. + Appl. Int. Soc. Opt. Photon., 66920M–66920M-14
Battistuzzi, F.U., Feijao, A., Hedges, S.B., 2004. A genomic timescale of prokaryote evolution: Insights into the origin of methanogenesis, phototrophy, and the colonization of land. BMC Evol. Biol. 4, 44–57.
Des Marais, D., 1998. Earth's early biosphere. Gravit. Space Biol. Bull.: Publ. Am. Soc. Gravit. Space Biol. 11, 23–30.
Des Marais, D.J. et al., 2002. Remote sensing of planetary properties and biosignatures on extrasolar terrestrial planets. Astrobiology 2, 153–181.
Domagal-Goldman, S.D. et al., 2014. Abiotic ozone and oxygen in atmospheres similar to prebiotic Earth. Astrophys. J. 792, 90–104.
Dressing, C.D., Charbonneau, D., 2013. The occurrence rate of small planets around small stars. Astrophys. J. 767, 95–114.
Dressing, C.D., Charbonneau, D., 2015. The Occurrence of Potentially Habitable Planets Orbiting M Dwarfs Estimated from the Full Kepler Dataset and an Empirical Measurement of the Detection Sensitivity. Available from: <arXiv: 1501.01623>.
France, K. et al., 2012. Time-resolved ultraviolet spectroscopy of the M-dwarf GJ 876 exoplanetary system. Astrophys. J. 750, L32.
France, K. et al., 2013. The ultraviolet radiation environment around M dwarf exoplanet host stars. Astrophys. J. 763, 149–163.
Gaidos, E., 2013. Candidate planets in the habitable zones of Kepler stars. Astrophys. J. 770, 90–101.
Gao, P. et al., 2015. Stability of CO_2 atmospheres on desiccated M dwarf exoplanets. Astrophys. J. 806, 249–260.
Goody, R.M., Yung, Y.L., 1989. Atmospheric Radiation: Theoretical Basis, second ed. Oxford Univ. Press, New York.
Harman, C.E. et al., 2015. Abiotic O_2 levels on planets around F, G, K, and M stars: Possible false positives for life? Astrophys. J. 812, 137–160.
House, C.H., Runnegar, B., Fitz-Gibbon, S.T., 2003. Geobiological analysis using whole genome-based tree building applied to the Bacteria, Archaea, and Eukarya. Geobiology 1, 15–26.
Hu, R., Seager, S., Bains, W., 2012. Photochemistry in terrestrial exoplanet atmospheres. I. Photochemistry model and benchmark cases. Astrophys. J. 761, 166–194.
Jin, Z. et al., 2014. Interannual variability of the Earth's spectral solar reflectance from measurements and simulations. J. Geophys. Res.: Atmos. 119, 4458–4470.
Kaltenegger, L., Traub, W.A., Jucks, K.W., 2007. Spectral evolution of an Earth-like planet. Astrophys. J. 658, 598–616.
Kasting, J.F., Whitmire, D.P., Reynolds, R.T., 1993. Habitable zones around main sequence stars. Icarus 101, 108–128.
Kharecha, P., Kasting, J., Siefert, J., 2005. A coupled atmosphere–ecosystem model of the early Archean Earth. Geobiology 3, 53–76.
Kopp, G., Lean, J.L., 2011. A new, lower value of total solar irradiance: Evidence and climate significance. Geophys. Res. Lett. 38, L01706. http://dx.doi.org/10.1029/2010GL045777.
Kopparapu, R.K., 2013. A revised estimate of the occurrence rate of terrestrial planets in the habitable zones around Kepler M-dwarfs. Astrophys. J. 767, L8.
Li, T., Tian, F., 2012. Detection of O_2 produced abiotically on habitable but lifeless planets around M-dwarfs. Proc. Int. Astron. Union 8, 39–45.
Liou, K.-N., 2002. An Introduction to Atmospheric Radiation. Academic Press.
Luger, R., Barnes, R., 2015. Extreme water loss and abiotic O_2 buildup on planets throughout the habitable zones of M dwarfs. Astrobiology 15, 119–143.
McLean, I.S. et al., 1998. Design and development of NIRSPEC: A near-infrared echelle spectrograph for the Keck II Telescope. Astron. Telesc. Instrum. Int. Soc. Opt. Photon., 566–578
Oke, J. et al., 1995. The Keck low-resolution imaging spectrometer. Publ. Astron. Soc. Pac., 375–385
Pierrehumbert, R.T., 2010. Principles of Planetary Climate. Cambridge University Press.
Ramirez, R.M., Kaltenegger, L., 2014. The habitable zones of pre-main-sequence stars. Astrophys. J. 797, L25.
Rein, H., Fujii, Y., Spiegel, D.S., 2014. Some inconvenient truths about biosignatures involving two chemical species on Earth-like exoplanets. Proc. Natl. Acad. Sci. 111, 6871–6875.
Rodler, F., López-Morales, M., 2014. Feasibility studies for the detection of O_2 in an Earth-like exoplanet. Astrophys. J. 781, 54–65.
Rothman, L. et al., 2013. The HITRAN2012 molecular spectroscopic database. J. Quant. Spectrosc. Radiat. Transfer 130, 4–50.
Rugheimer, S. et al., 2015. Effect of UV Radiation on the Spectral Fingerprints of Earth-like Planets Orbiting M dwarfs. Available from: <arXiv:1506.07202>.
Segura, A. et al., 2005. Biosignatures from Earth-like planets around M dwarfs. Astrobiology 5, 706–725.
Tian, F., Ida, S., 2015. Water contents of Earth-mass planets around M dwarfs. Nat. Geosci.
Tian, F. et al., 2014. High stellar FUV/NUV ratio and oxygen contents in the atmospheres of potentially habitable planets. Earth Planet. Sci. Lett. 385, 22–27.
Tuomi, M. et al., 2014. Bayesian search for low-mass planets around nearby M dwarfs–estimates for occurrence rate based on global detectability statistics. Mon. Not. R. Astron. Soc. 441, 1545–1569.
Turnbull, M.C. et al., 2006. Spectrum of a habitable world: Earthshine in the near-infrared. Astrophys. J. 644, 551–559.
Vogt, S.S. et al., 1994. HIRES: The High-Resolution Echelle Spectrometer on the Keck 10-m Telescope. In: 1994 Symposium on Astronomical Telescopes & Instrumentation for the 21st Century. International Society for Optics and Photonics, pp. 362–375.
Walker, J.C., 1977. Evolution of the Atmosphere. Macmillan, New York and Collier Macmillan, London, p. 1.
Wolf, E., Toon, O., 2015. The evolution of habitable climates under the brightening Sun. J. Geophys. Res.: Atmos. 120, 5775–5794.
Wright, G.S. et al., 2004. The JWST MIRI instrument concept. SPIE Astron. Telesc. + Instrum. Int. Soc. Opt. Photon., 653–663
Yang, J., Cowan, N.B., Abbot, D.S., 2013. Stabilizing cloud feedback dramatically expands the habitable zone of tidally locked planets. Astrophys. J. 771, 45–51.